Impact of Oscillatory Movement on Insulation Reliability of Cables Supplying Offshore Platforms

FF2020-1011

Dr Christopher Emersic
Miss Frances Hu
Dr Tony Lujia Chen
Prof Simon Rowland

25/08/2022

Summary

This report outlines progress examining the impact of in-service oscillatory movement on insulation reliability of AC and DC cables serving offshore platforms. The study ran between Dec 2020 to Jul 2022 and investigated whether repeated flexing of a cable may significantly reduce a cable's life expectancy through repeated extension and compression of the polymeric dielectric, with particular focus on electrical tree growth. The study consisted of three main work packages, investigating (a) the impact of bulk conductivity changes that occur with changes to insulation strain, (b) the impact of strain on tree growth and inception behaviour, and (c) whether testing at laboratory scales is representative of larger cables.

No clear relationship was found between the levels of strain up to an order of magnitude greater than likely seen in cables in service and steady-state current measured, indicating changes in tensile stress do not significantly influence volume conductivity. The geometry of electrical trees was observed to be significantly affected by tensile strain, which acted to produce much straighter and narrower trees. Initiation time and growth rate were not affected by tensile strain, suggesting lifetime may not be affected. Utilising ORE Catapult's dynamic cable bend fatigue rig in Blyth, testing that combined concurrent mechanical flexing and electrical treeing revealed comparable results to those observed in the laboratory, supporting the representativeness of laboratory scale testing.

Table of Contents

MANCHESTER 1824
The University of Manchester

1 Introduction

Offshore wind energy is central to UK's ambition of reducing carbon emissions. The growth of power generation from wind farms increasingly further from shore in deeper waters requires greater reliability from the connecting power cables. The Floating Wind Joint Industry Project Report 2018 identified cables to be at the heart of priority innovation needs [1]. Typically, cable assets contribute to 5–10% of the total investment costs for an offshore wind farm, yet cable failures cause the majority of the offshore power outages and account for approximately 80% of insurance claims in this industry [2]. In deeper waters, wind turbines are often floating and the cables buoyant. This increases the mechanical strain the dielectric insulation is subjected to, which is enhanced further by flexing caused by tidal and wave motion. Cables could suffer irreversible damage through long periods of operational mechanical flexing, leading to accelerated ageing through mechanisms such as electrical treeing, thereby shortening service lifetime. There is little knowledge on the consequences of low frequency flexing, or repeated compression and extension of cable insulation because cables are typically installed in relatively benign environments.

The project will explore whether flexing a cable significantly reduces the cable's life expectancy through repeated extension and compression of the polymer dielectric. In particular, the impact of dynamic strain on the electrical tree growth failure mechanism will be explored. Electrical treeing is a phenomenon in which microscopic tree-like gaseous channels grow within the dielectric insulating material of a cable in the presence of a field [3]. Electrical trees can lead to a short circuit through the bulk insulation causing catastrophic cable failure [4]. There are limited studies examining the influence of compressive strain on electrical trees and very few documenting the influence of tensile strain [5]–[8], with observations showing a strong influence on tree geometry.

Most offshore cables are operated under AC voltages, but more installations of DC cables are expected in the future. Under AC voltages, the electric field within solid insulation material, such as low-density polyethylene (LDPE), is driven by its permittivity. Under DC voltages, conductivity is a dominating factor. Conductivity is strongly dependent on temperature and electric field, with a well-established relationship deriving from a hopping theory model of conduction in dielectrics (e.g., Boggs et al., 2001 [9]). In XLPE, conductivity can increase by two orders of magnitude between 20 to 80°C, although the influence of electric field is much smaller and typically acts to reduce the magnitude of the temperature effect.

The dielectric materials used in floating power cables supplying offshore wind can be subjected to oscillatory changes in mechanical strain. When carrying DC currents, it is not known whether such mechanical changes under DC fields cause corresponding conductivity changes resulting from the compressive and tensile forces altering material charge trap depth and density. These mechanically driven changes may yield an equivalence with a mechanically static system under the influence of an AC voltage. If so, mechanical flexing of insulation could give AC-like fields despite using DC voltages. This is of concern because the phenomenon of electrical treeing is known to be more aggressive under AC conditions. Section 2 describes this investigation, and the influence of strain on electrical tree behaviour is discussed in section 3. Section 4 investigates the representativeness of laboratory scale testing on larger scale cables.

2 Conductivity variation with mechanical strain

Steady-state volume conductivity through a polymeric dielectric under strain was a challenging measurement and considerable preparatory and pre-trial experimentation was required before the measurement could be made successfully and repeatably. The final revision of the process is described here.

2.1 Experimental setup

Experimental testing of changes in insulation DC volume conductivity with tensile stress was conducted using an arrangement as shown in Figure 1. Two materials were used to make low density polyethylene (LDPE) samples: Lupolen 2420 H forged in a hot press, and Aldrich GF12363735 produced by extrusion from a third-party manufacturer. Both materials have densities of density 0.92 g cm^{-3} and dielectric strength of 27 kV mm^{-1}. Materials were not thermally treated prior to testing. Samples were housed in a custom-built stretching rig (Figure 2). Rectangular samples 100 mm long, 50 mm wide, 0.5 mm depth, were secured within the rig to apply extension. After tensile strain was applied, samples were sandwiched within a three-electrode configuration commonly used to measure volume currents (Figure 3) and raised to potentials of up to 5 kV. Current passing through the bulk insulation to earth was measured using a sensitive Keithley Picoammeter 6485 capable of measuring to 10 fA. Electrical noise levels were minimised to 2–4 pA by performing the experiments in an earthed faraday cage. In the three-electrode configuration, the earth terminal is surrounded by a guard electrode following the design specified in BS 6233 [10] to capture stray currents and ensure the measurement reflects currents passing through the bulk material alone. Measurements of steady-state volume current density were made as a function of applied voltage and extension.

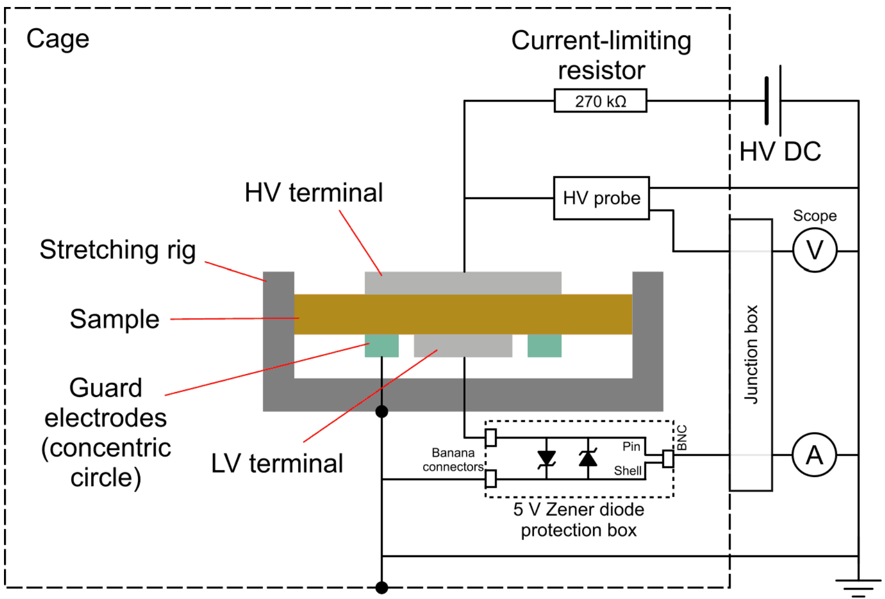

Figure 1. Experimental setup and circuit diagram for steady-state conductivity measurements.

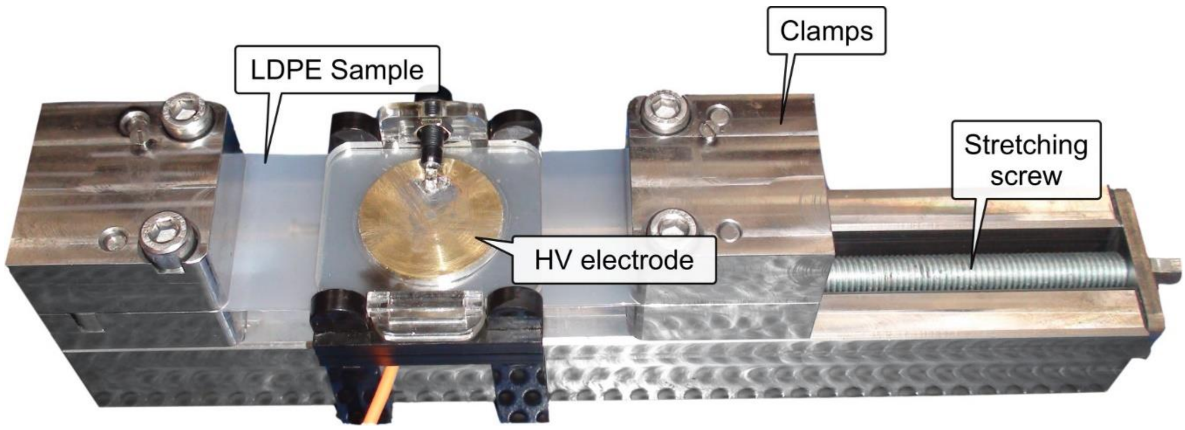

Figure 2. Custom-built sample stretching rig to apply known percentage extensions to LDPE samples. Distance is measured using Vernier callipers.

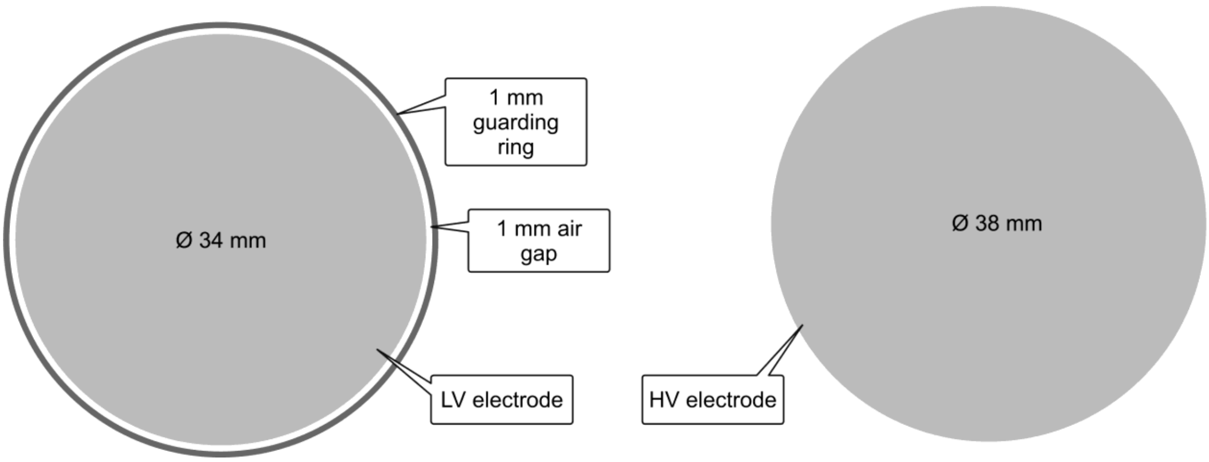

Figure 3. Sketch of electrode dimensions.

2.2 Conductivity results

Figure 4 shows typical measured currents through LDPE of thickness 0.5 mm, without strain, as a function of voltage. Steady-state current was achieved after approximately 20 minutes. There is a clear relationship between the decay profile and the resulting steady state current as a function of voltage, with higher voltages and the associated electric field strength resulting in the largest currents.

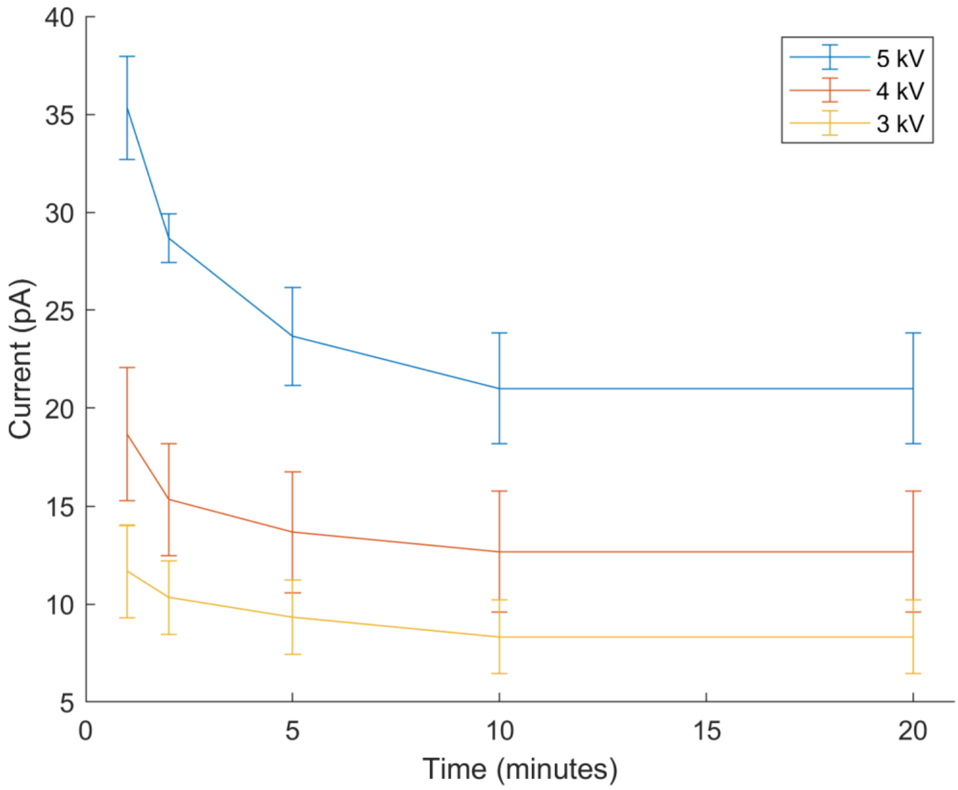

Figure 4. Example of typical current response measured through samples, with measurement standard deviation shown.

The steady-state currents in Figure 4 are plotted as a function of voltage in Figure 5 and show a superlinear trend. The steady-state current density is determined by taking the ratio with the surface area of the electrode, and volume conductivity is achieved by normalising against the electric field strength. The volume conductivity as a function of voltage (Figure 6) mirrors the superlinear trend observed with the current, with values within a factor of 2 over the voltage range tested. The volume conductivity does not change significantly as a function of tensile strain (Figure 7).

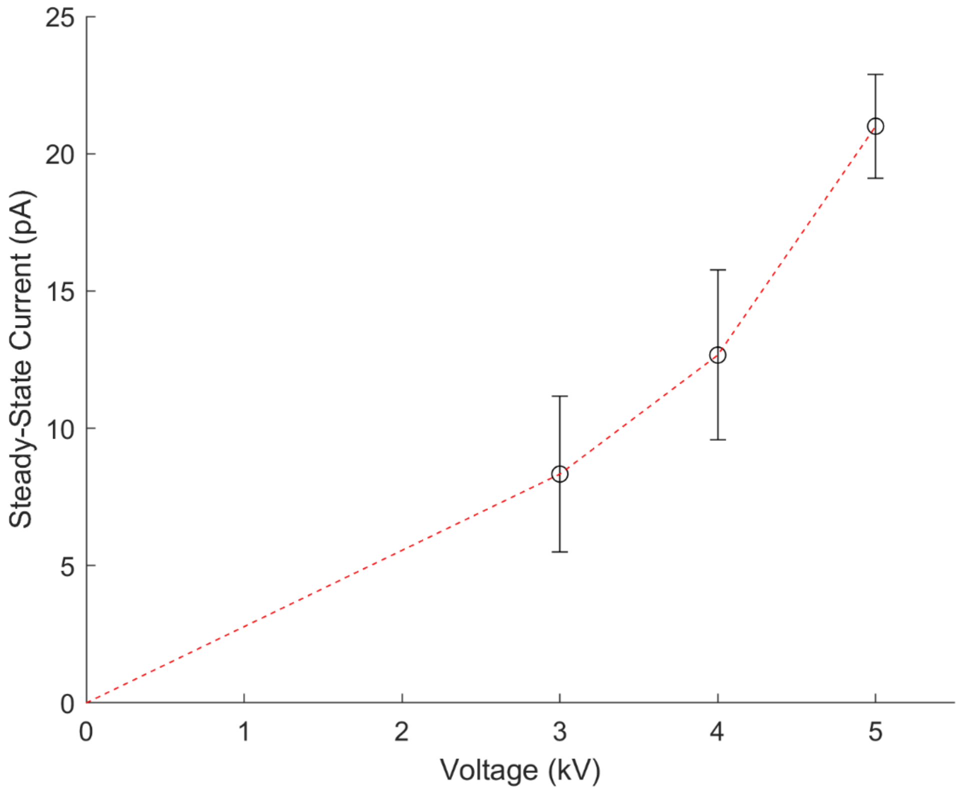

Figure 5. Mean steady-state current plotted as a function of applied voltage across a 0.5 mm LDPE sample, with standard deviation and trend line in red shown.

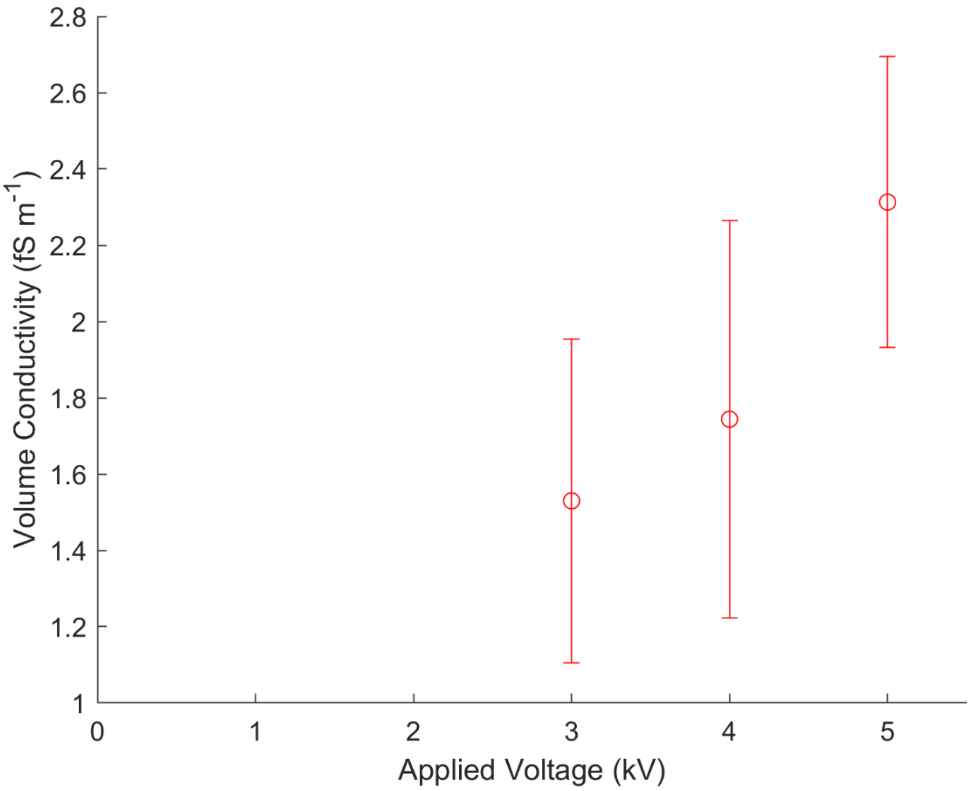

Figure 6. Mean volume conductivity as a function of applied voltage with standard deviations shown.

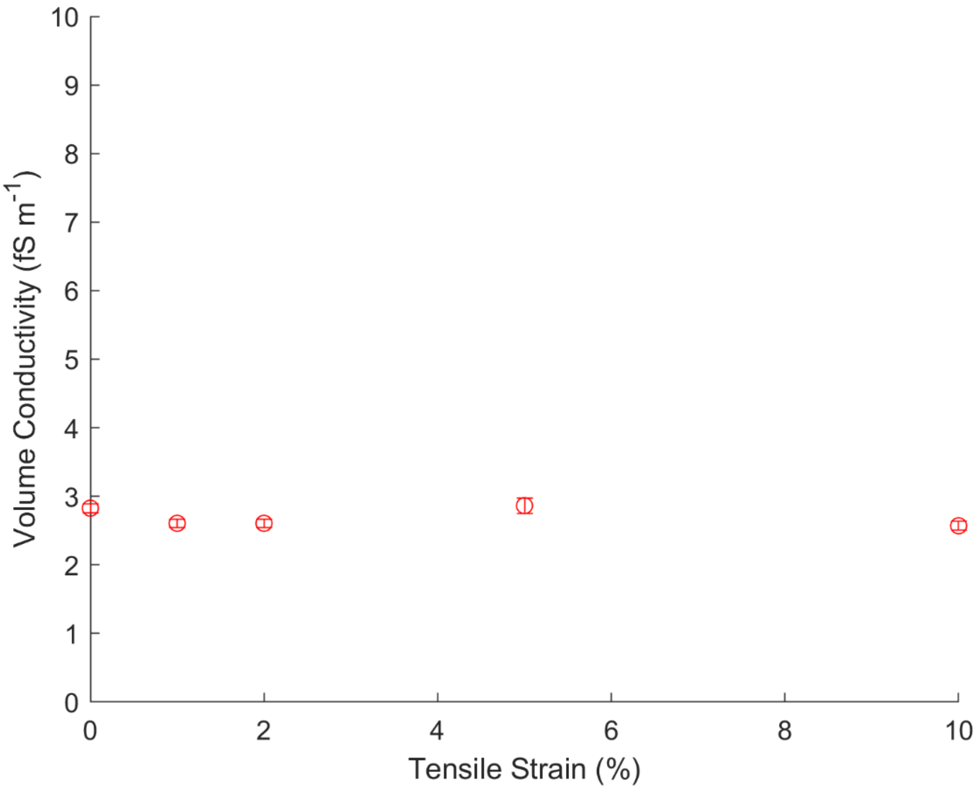

Figure 7. Volume conductivity as a function of tensile strain at 5 kV with standard deviations shown.

2.3 Discussion

Current is driven through the bulk polymer insulation in the presence of an electric field. Initially, both polarisation and conduction currents flow, but the polarisation current component readily decays to leave only the desired steady-state conduction current, as observed in Figure 4. The current decay profile is consistent with other studies [11] indicating the system is responding as expected and that steady-state current is ultimately being measured.

It was not possible to measure steady-state currents below 3 kV with the equipment used, and it is assumed that in the absence of an electric field, there will be no significant current (Figure 5). Unlike Ohm's law with conductors, where resistance is near zero and not dependent on electric field strength, with dielectrics, resistance is likely to decrease with increasing electric field strength, producing a nonlinear current response as observed.

Reported values of conductivity for polyethylene in the literature range between 1 and 100 fS m^{-1} [12]. Values observed here fall within that range at approximately 2 to 3 fS m^{-1} (Figure 7). The variability between the measured values of volume conductivity for a range of voltages and material thicknesses is within a factor of two, which is small relative to the two orders of magnitude variation reported in the literature. There is no apparent relationship between volume conductivity and tensile strain up to values of 10%, which is approximately an order of magnitude greater than considered an operational maximum experienced by in-service cables, based on modelling by industry partners.

Many studies have determined volume conductivity using very thin samples of the order of tens of micrometres [12]–[16]. Given charge injection and the influence of charge mobility in dielectrics, it is not clear whether the conductivities determined from such thin samples in the literature are representative of bulk material behaviour. While samples used here have thicknesses greater than 100 µm [17], considered to be a reasonable transition thickness from thin film to bulk behaviour, further investigation is required to confidently establish whether the measurements of volume conductivity acquired are representative of the bulk, rather than reflecting interfacial effects associated with space charge deposition and removal.

3 Characterising tree growth in polyethylene with mechanical strain

This project explores the potential for enhanced risk to deep water cables from repeated extension and compression of the polymer dielectric of a cable, and whether this significantly reduces its life expectancy, with particular focus on the impact on electrical tree growth. There are limited studies examining the influence of compressive strain on electrical trees [7]. Many of these rely on residual internal strain left over from cooling processes which is also seen in the cable structure. Very few studies have documented the influence of tensile strain; however, its influence on electrical trees has been studied in [5]–[8]. Observations typically show tensile strain reduces breakdown strength of XLPE [5] and affects tree initiation time [6]. Strain is suggested to affect the molecular bonding of insulation, modifying the breakdown pathways, with compressive strain likely hindering tree propagation [7]. Here, cross-linked polyethylene (XLPE) is extracted from extruded 66 kV power cables and subjected to electrical tree growth as a function of tensile strain levels representative of those found in service.

3.1 Experimental setup

The experimental arrangement for growth of electrical trees is shown in Figure 8. A balanced circuit (Figure 9) was used to minimise background electrical noise and maximise detection of partial discharge signals associated with tree growth [ref]. Samples were produced by extracting the XLPE insulation from 66 kV power cables and slicing into half-rings of 3 mm thickness. Needles with 3 µm tip radius were inserted into the centre of the samples leaving a gap distance of 2 ± 0.1 mm between an earthed plane electrode (Figure 10(a)). This was achieved by heating both needle and XLPE sample material to 140°C in an oven prior to needle insertion, which minimises the likelihood of needle tip damage and air gaps between the needle tip-insulation interface. An 80 kV_{RMS} transformer fed through a Thurlby Thandar TG215 2 MHz function generator and Europower EP4000 amplifier supplied a bipolar sinusiodal 50 Hz AC voltage to 50 mm needles with 3 µm tip radius manufactured by Ogura Jewel Industry Co., Ltd. Voltage was applied, increasing at a rate of 500 $V_{rms}\,s^{-1}$ to 7.5 kV_{rms} to achieve a calculated peak field around the needle tip of 895 $kV\,mm^{-1}$ following Mason's equation which assumes no space charge accumulation [18]. A PD-free sample, otherwise identical to those to be tested, was fabricated using a needle with a 500 µm rounded tip and used as part of a balanced circuit with an Omicron MPD 800 system, in accordance with IEC 60270 [19], to minimise background noise. Calibration was conducted with an Omicron CAL

542, with sensitivity of approximately 1 pC. An overcurrent relay and 500 kΩ current-limiting resistor were used to protect the test equipment in the event of a breakdown. Trees were allowed to grow for 2 hours, and optically imaged on completion of the test using a Keyence VHX 7100 microscope. Tree growth was recorded periodically using a Manta G-507B CCD camera and backlight to measure growth rate during energisation.

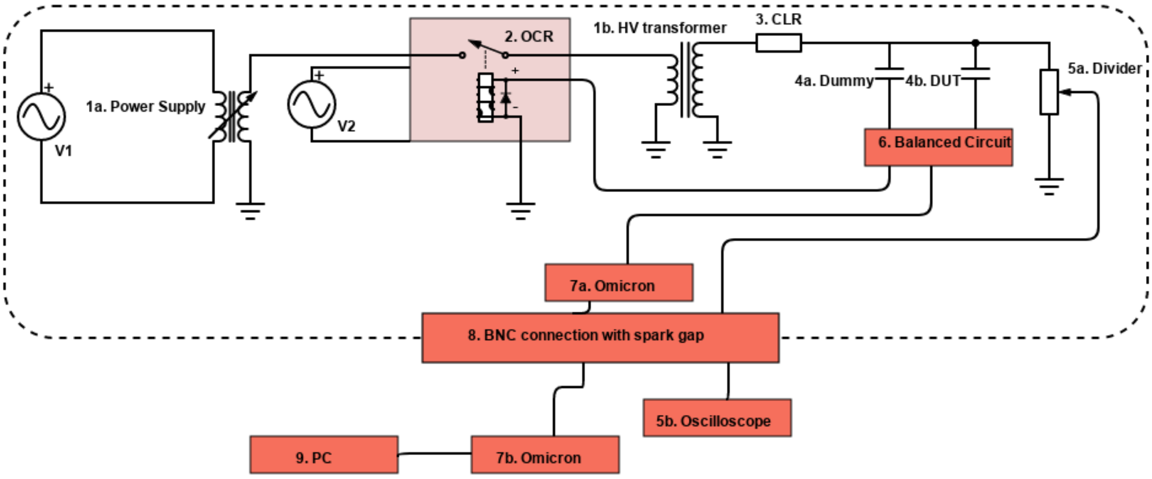

Figure 8. Experimental setup for circuit diagram for tree growth experiments.

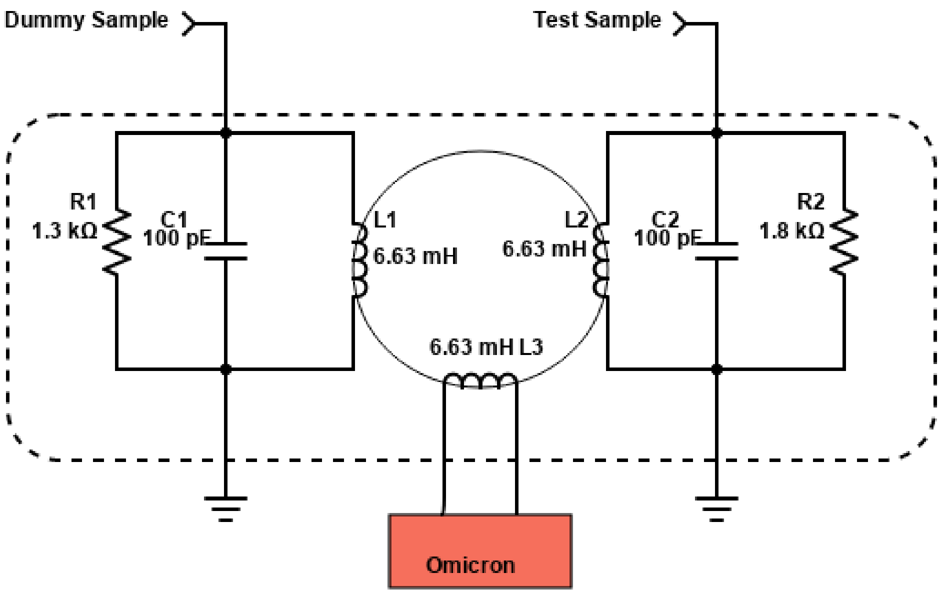

Figure 9. Balanced circuit for treeing experiments.

Tensile strain was applied to samples using a mechanical rig shown in Figure 10(b). Modelling of the samples using ANSYS engineering simulation and 3D design software suggests the volume in which the tree grows will experience strain as shown in Table 1. The half-ring geometry of the samples allows global compression from the top edges shown in Figure 10(b) to generate tensile strain around the needle tip shown in Figure 10(b). Electrical trees were optically recorded using a video camera and later examined under a microscope.

Table 1. Edge compression required to achieve tensile strain around needle tip

Global compression (mm)	Corresponding tensile strain around needle (%)
0.95	1.1
2.31	2.7
4.69	5.5

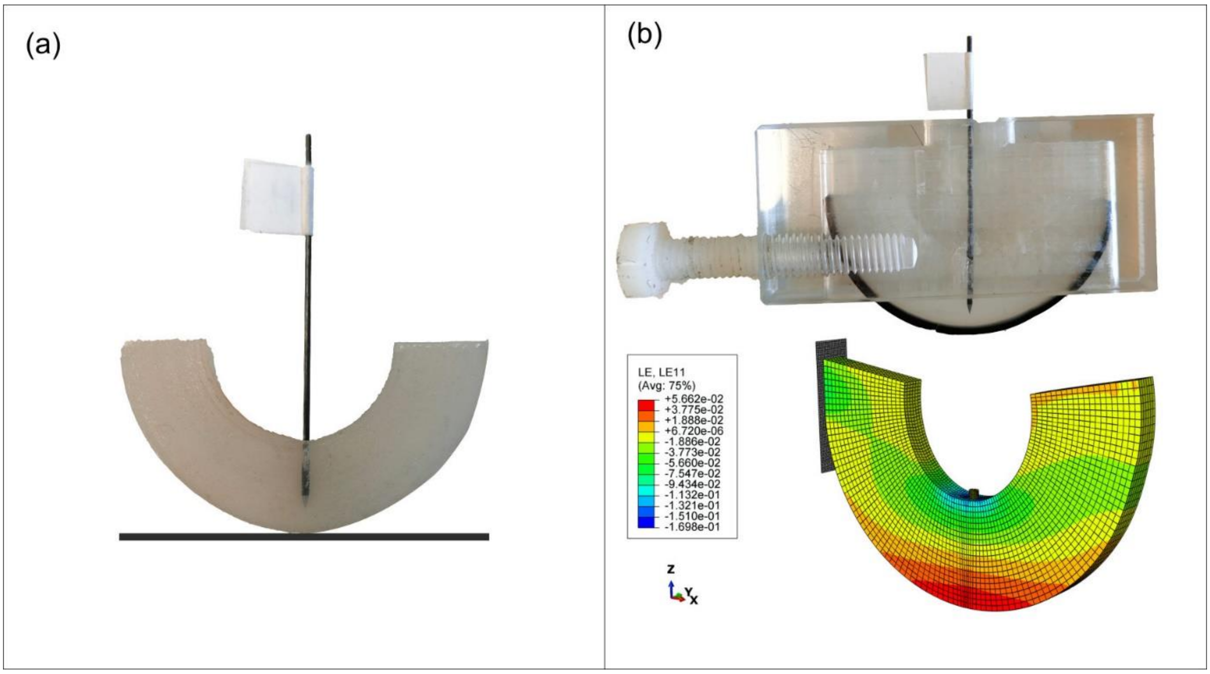

Figure 10. (a) Needle-plane sample of XLPE, (b) Rig to apply tensile strain around needle tip and example of computed strain profiles.

3.2 Electrical treeing results

Increasing tensile strain was observed to decrease the width and aspect ratio of resulting trees (Figure 11). Quantification of this was achieved by analysing the growth rate and angles of the tree branches. Figure 12 shows the mean tree growth rate as a function of tensile strain. Growth shows the typical inverse sigmoid profile commonly observed; however, no relationship was observed with tensile strain.

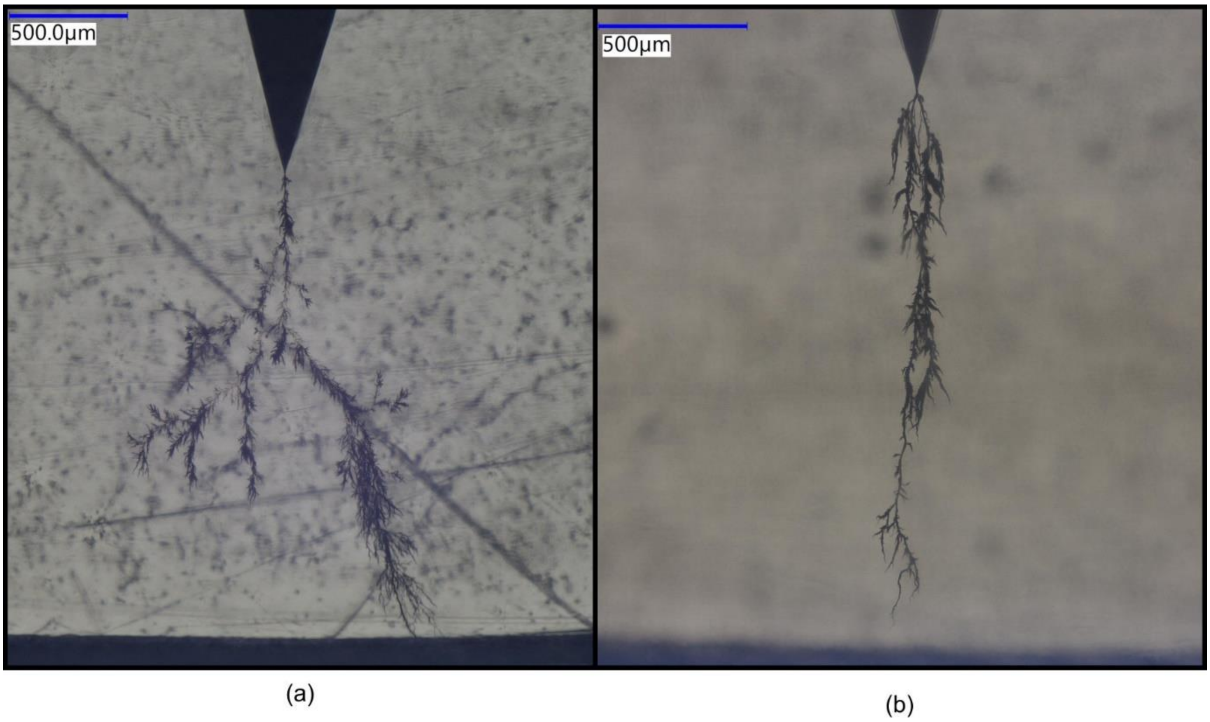

Figure 11 Typical example trees for (a) no strain and (b) 10% tensile strain, at 7.5 kV_{rms} with a gap size of 2 mm.

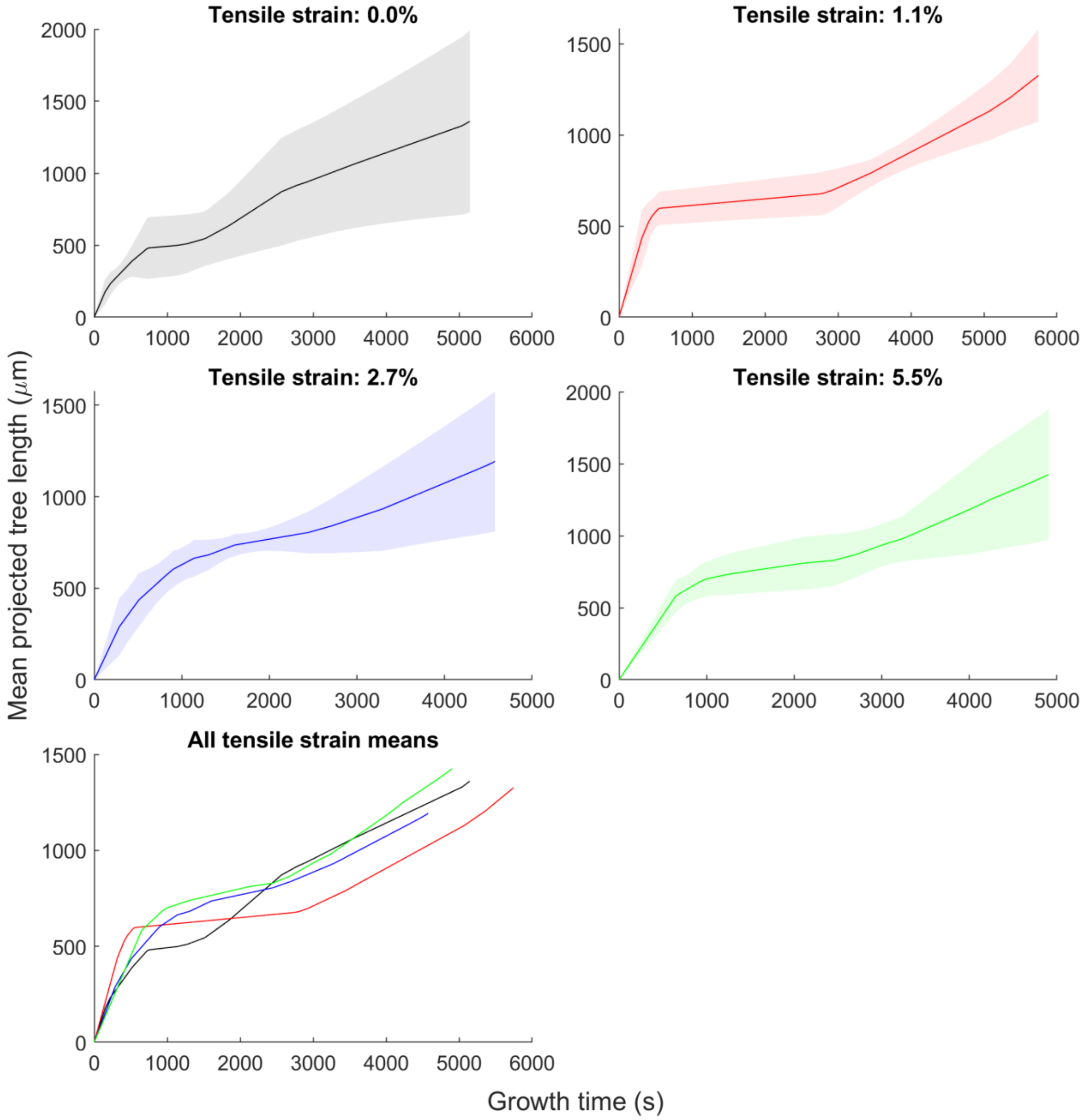

Figure 12. Mean tree growth rate as a function of tensile strain. Shaded regions denote standard deviation.

The mean height-to-width ratio of the trees (Figure 13) shows a clear reduction in width with increasing tensile strain, particularly at higher strains.

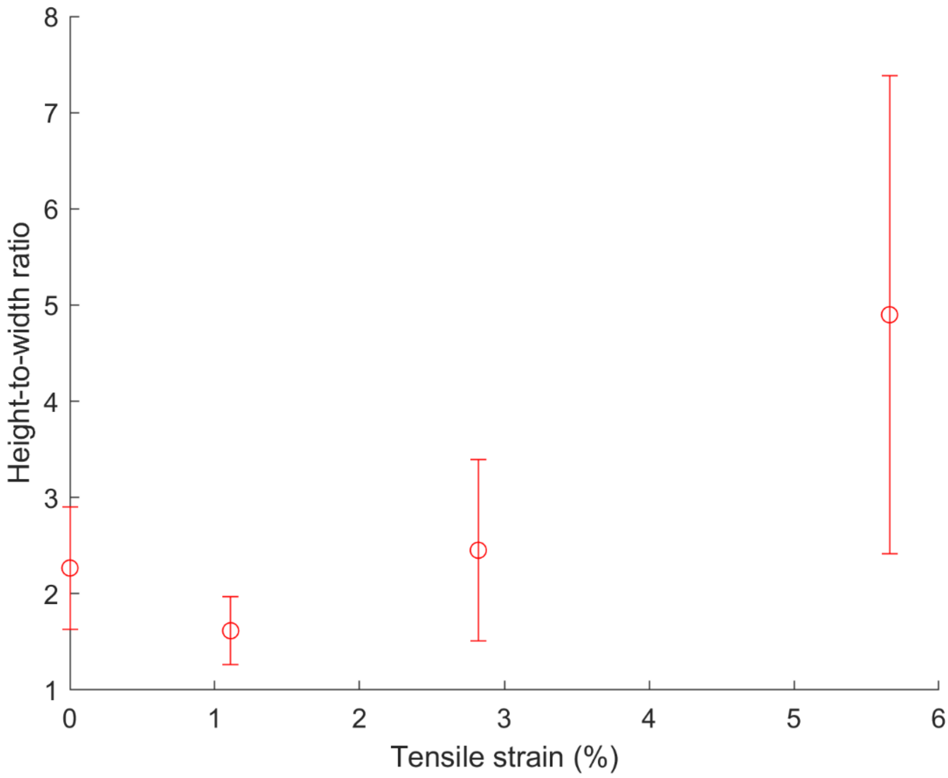

Figure 13. Mean height-to-width ratio of trees as a function of tensile strain with standard deviations shown.

Figure 14(a) shows a normalised histogram of the bend and bifurcation angles of the main channels of the trees (Figure 15). The relationship with tensile strain is illustrated more clearly with coarser bins, reflecting shallow and acute angles as shown in Figure 14(b). The distribution relationship as a function of tensile strain is nonlinear, with accelerating likelihood of reduced tree width as strain increases (Figure 14(c)), consistent with observations of the dimensional geometry shown in Figure 13.

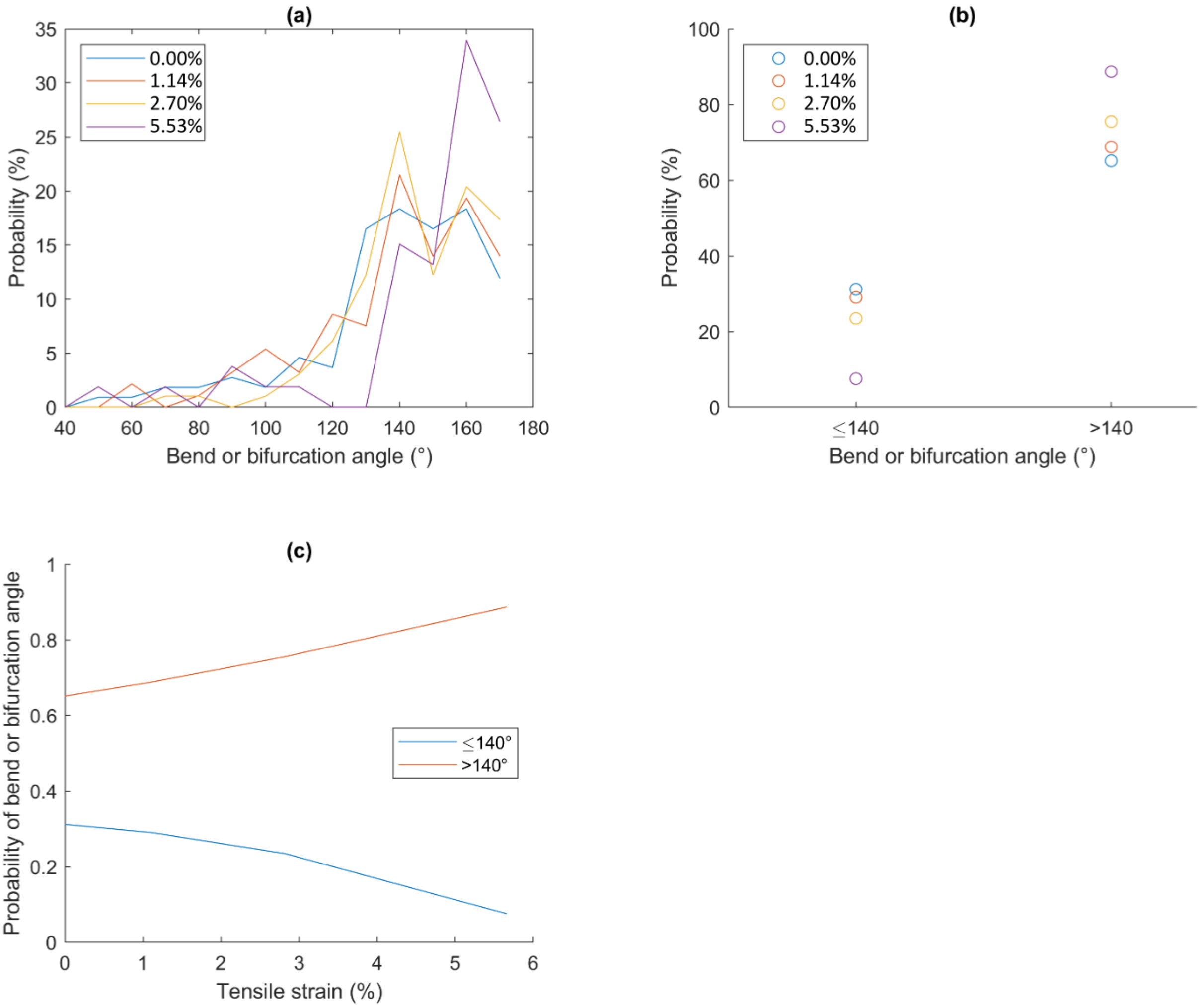

Figure 14. (a): Normalised histograms of tree bend and bifurcation angles as a function of tensile strain; (b): As (a) except binned more coarsely; (c): Probability profile of (b) as a function of tensile strain.

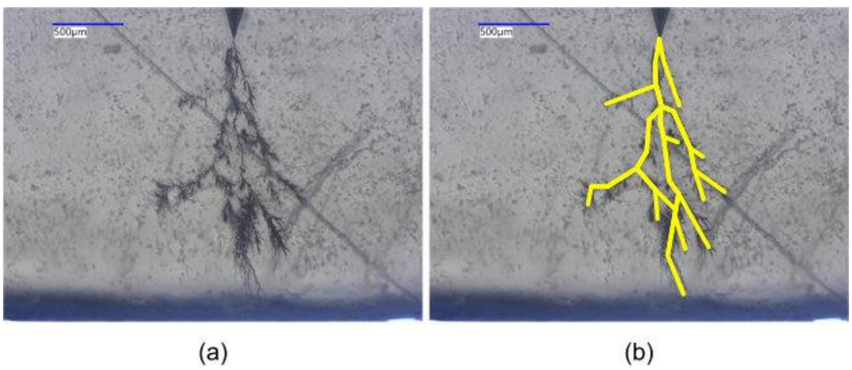

Figure 15. Example illustration of how main channels of tree image (a) were approximated (b) to measure bend and bifurcation angles.

An electrical tree produces an ordered but varied geometrical, fractal-like pattern. The density of the branches can be described by the fractal dimension of the object. The total length of all elements making up the fractal object is related to its height by a power law relation (1).

$$S_n \propto L^{d_f} \tag{1}$$

where, S_n is the total length of all elements d_i (2) in the fractal object, L is the height of the fractal tree, and d_f is the fractal dimension (index of the power relation)

and

$$S_n = \sum_{i}^{n} d_i \tag{2}$$

A box-counting method [20] was used to quantify over what spatial resolution range the computed fractal dimension relation held, from analysis of a two-dimensional projection of the 3D tree object, and the fractal index was determined. The mean fractal dimension for all strains was 1.96 ± 0.03, indicating that the branch density is unaffected despite substantially different tree geometries.

Mechanical strain was applied uniaxially along one dimension. While this was observed to influence the width of the trees, the extent of the branches was not expected to vary as a function of sample thickness (the y-axis of Figure 10 (b)) since strain is uniform across that dimension. Measuring the z-depth of the tree branch penetration by sweeping the focal plane under the microscope revealed the mean z-depth to be around 1100 ± 100 µm for all applied tensile strains, indicating no relationship.

The initiation time of the trees showed no evidence of being affected by the application of tensile strain, with trees initiating within 10 minutes with mean time of 4 minutes (Figure 16). Trees initiation time was stochastic with some initiating immediately after energisation. Partial discharge activity shows three typical distinct stages (Figure 17). Initially, phase-symmetric but amplitude asymmetric discharges increase in magnitude with phase and correlate with the rising externally applied field. These discharges peak in magnitude at approximately 300 pC and correlate with initial growth of trees from the needle. This growth can vary in physical length to near the full gap distance. Growth stagnation follows and partial discharge activity stops. After a varying delay, significant growth begins again from offshoots of one or more of the original principal branches. This does not correlate with significant partial discharge activity, which often remains low in magnitude. As this secondary growth nears the earth plane, partial discharge magnitude correspondingly increases and shows a polarity and phase-symmetric profile. Discharge magnitude increases with the waveform rising edge and decreases with field, and peak magnitudes are typically lower than initially, with the bulk being less than 10 pC until near breakdown. This behaviour is seen in all trees grown at different tensile strains, indicating strain does not appear to be significantly influencing the electrical behaviour despite influence on the tree geometry.

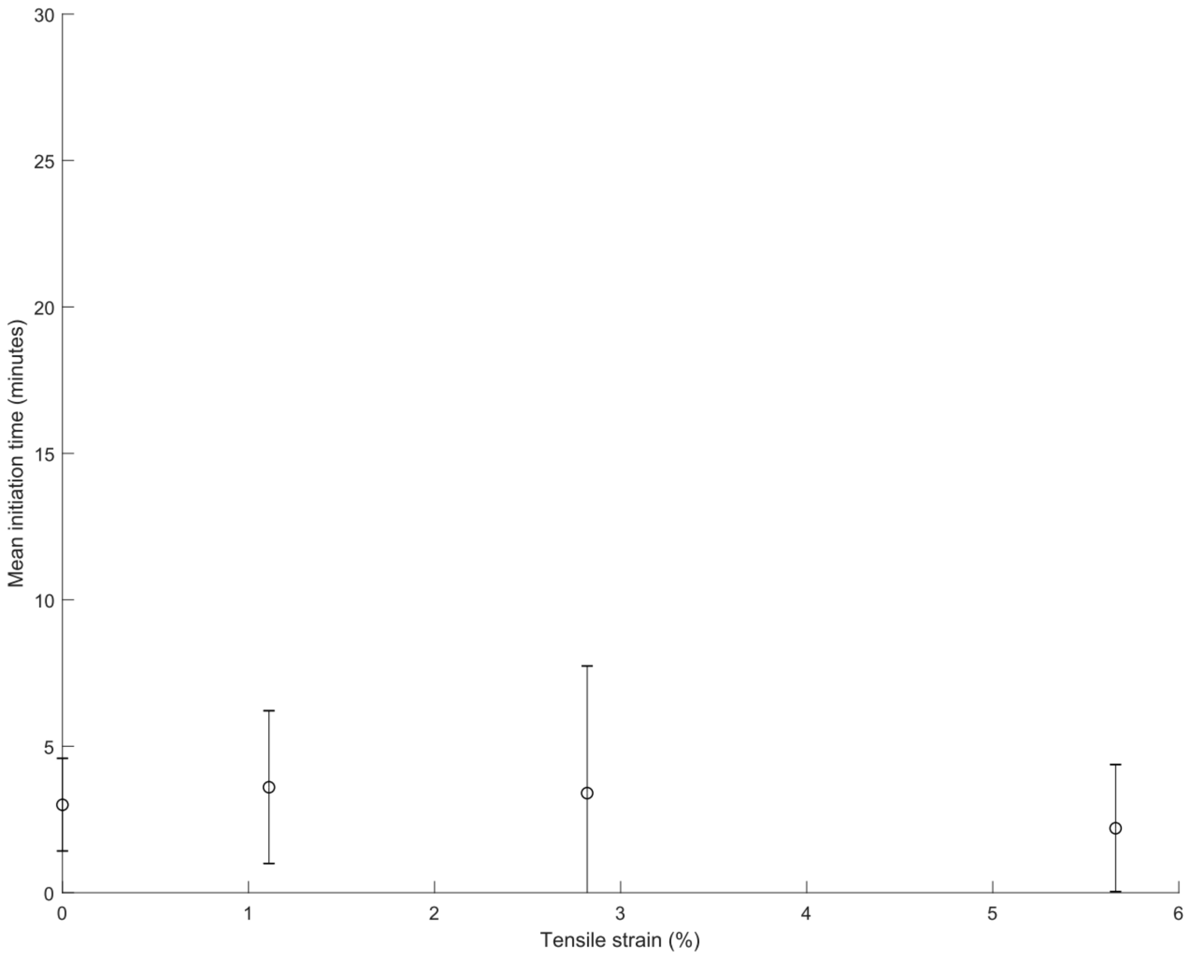

Figure 16. Relationship between the mean tree initiation time as a function of tensile strain with standard deviations shown. In some tests, initiation occurred immediately after energisation.

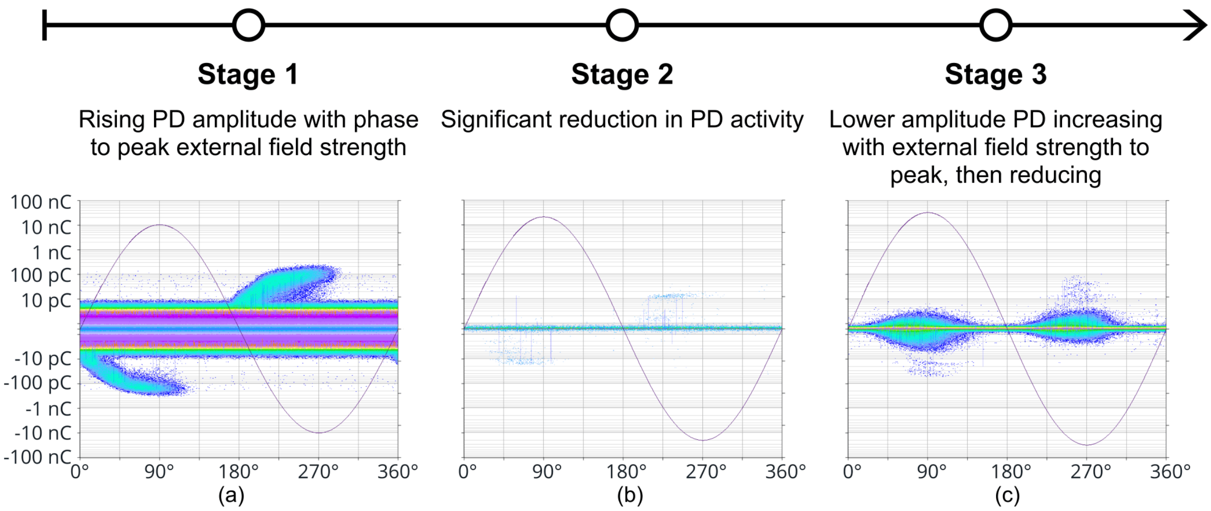

Figure 17. Typical stages of partial discharge activity during tree development

3.3 Discussion

The observed decrease in tree width with increasing tensile strain is consistent with limited studies in the literature. David et al., 1996 [8] mechanically pre-strained XLPE and allowed relaxation, showing a reduction in tree length after a given growth time with increased tensile strain. Du et al., 2018 [21], observed increasing compressive strain affected tree propagation characteristics and increased effective tree width for EPDM rubber. They argued compressive strain reduced the free volume of microvoids, reducing the mean free path of electrons during the partial discharge process, although no partial discharge measurements were reported. Our observations did not show fundamental change in the partial discharge behaviour as a function of tensile strain. Increasing tensile strain may thus not have the opposite effect and increase the free volume of microvoids. Strain influences and modifies the breakdown pathways, apparently affecting the tree geometry [7], but not growth rate (Figure 12) or density of branches formed, as measured by the fractal index.

Initiation time was not observed to be influenced by tensile strain, in contrast to Champion et al., 1994 [6], who found tensile strain reduced initiation time. However, synthetic resin was used, which is materially very different to XLPE examined here. This suggests that the application of strain may not pose greater risk to the severity of treeing events or correspondingly reduce service lifetime. Additionally, with respect to in-service applications, the observed influence of strain became noticeable in trends at a value of 5.7% (Figure 13, Figure 14(c)). Discussions with industry partners that modelled cables in service suggest maximum experienced strains are likely to be approximately 1%. Many studies which have examined the influence of externally applied strain in other materials have used values considerably greater than this in the tens of percent (e.g., [21], [22]) and so may not be directly applicable to real-world applications.

The characteristic evolution of partial discharge in three stages does not correlate with the physical tree growth. While there is stochastic variability between trees, significant growth was observed at times when little partial discharge activity was observable. This indicates that high amplitude partial discharge alone is not always directly driving tree propagation.

In summary, there was an observed relationship between tree properties and geometry, with increasing tensile strain producing narrower trees, but not influencing the characteristic partial discharge evolution. Despite the geometric change, the branch density and time to failure remained unaffected by tensile strain.

4 Comparison between small-scale and large-scale electrical and mechanical testing

ORE Catapult's dynamic cable bend fatigue rig in Blyth as shown in Figure 18(a) was used to conduct tests combining mechanical flexing and electrical treeing concurrently on 66 kV power cable samples. The primary aim was to examine whether observations on the small scale translate to larger scale testing on real-world samples. Three principal tests were conducted with cable samples: unstrained conditions, statically strained, and dynamically strained. Such testing was somewhat adventurous, given the novelty of the approach, and was a significant learning experience. The authors are grateful to Aidan Ebrahim, Alex Neumann, Will Brinley, Kevin Leigh, and the rest of the ORE Catapult team for their support.

4.1 Experimental setup

66 kV power core cables approximately 5 m in length were used as test samples shown in Figure 18(b). Ends were prepared as shown in Figure 18(c) by exposing the core, stripping back the semiconductive layer to prevent surface flashover, and earthing the screen. Brass end caps were placed over the core ends to minimise peak fields and silicone sealant was used at the cap-cable interface to eliminate small air gaps and corona (Figure 18(f)). A hole with 1 cm in diameter nearer the centre of the cable length was drilled through the outer sheath and screen to a depth sufficient to reveal the insulation layer (Figure 18(d)). A square-ended drill bit was used to minimise insulation penetration. Cables were heated using a heating blanket to reach 70°C (Figure 18(e)). A rig was used to insert a needle of identical specification given in Section 3.1, centrally into the drilled hole. The needle was heated to 140°C using a modified soldering iron and needles could be inserted normal to the surface to a depth sufficient to give an approximate gap size of 2 mm between the needle tip and semiconductive layer covering the core. This depth was gauged beforehand. This process of sample preparation was as similar as possible to that for small scale lab samples described in Section 3.1.

Cables with needles inserted were crane-lifted onto the large bend rig. The centre of the cable length was placed across the centre of a lower former of bend radius 2.5 m, giving tensile strains of approximately 1%, and ratchet strapped down. The ends were placed through the rig's collars (Figure 18(g)) and cleats were used on both sides of the collar on one end of the cable to secure it to the rig and prevent horizontal sliding during flexing (Figure 18(h)). This was necessary because the cores have smaller diameter than the larger parent cables the rig was designed for. The secured end not subjected to flexing was connected to the circuit; the core was connected to high voltage via a hole drilled in the end cap for a standard 4 mm banana lead, and the screen was earthed (Figure 18(f)). The other end of the cable was free to be subjected to bending by the rig. The hole and needle were positioned to be in a region of the cable that was above the former and away from the centre where it was ratchet strapped (Figure 18(i), Figure 19). The rotation of the cable in the rig was such that the hole and needle pointed upwards, normal to cable's surface. Needles were connected to earth.

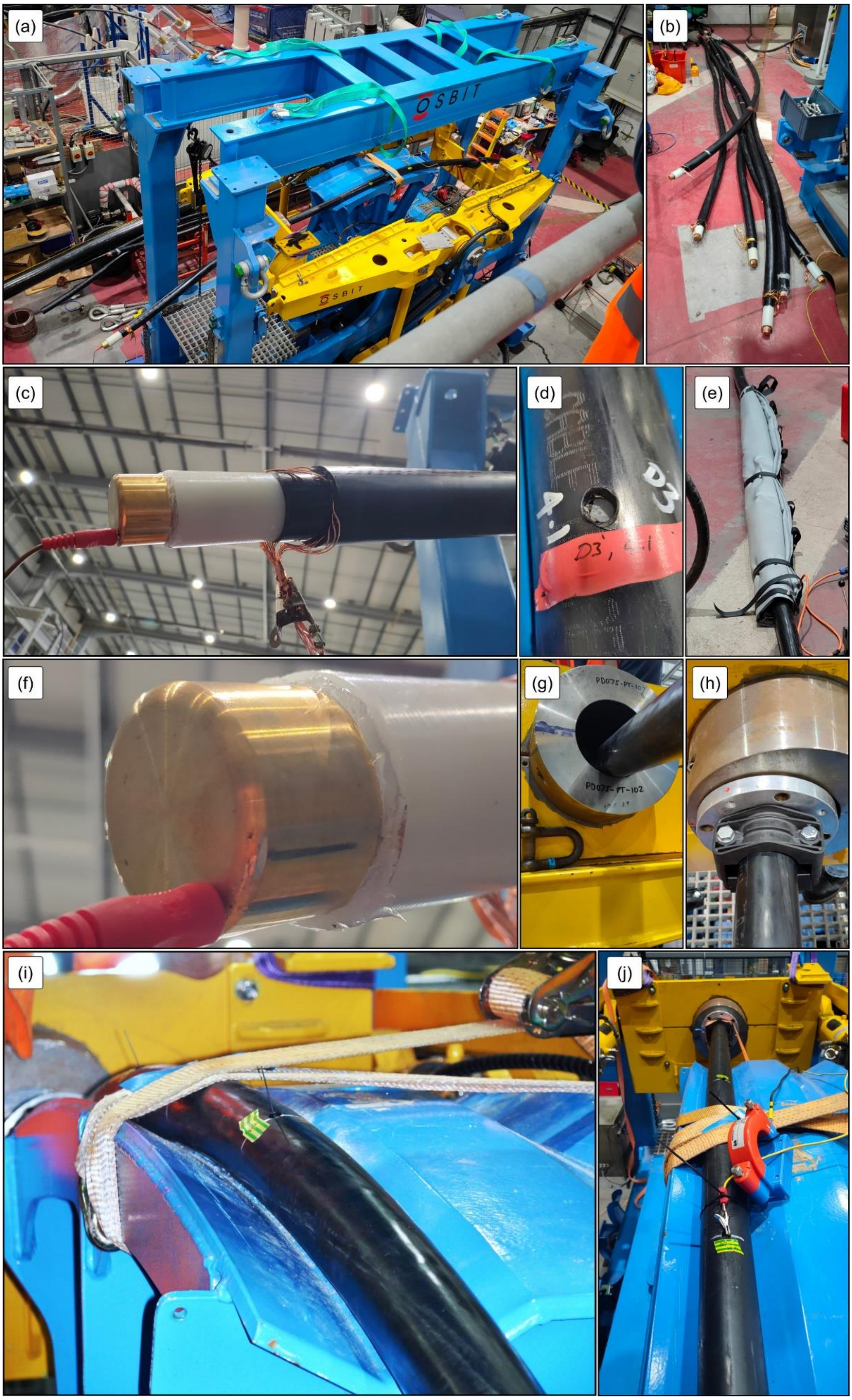

Figure 18. Various images of the test setup (descriptions provided in main text of section 4.1).

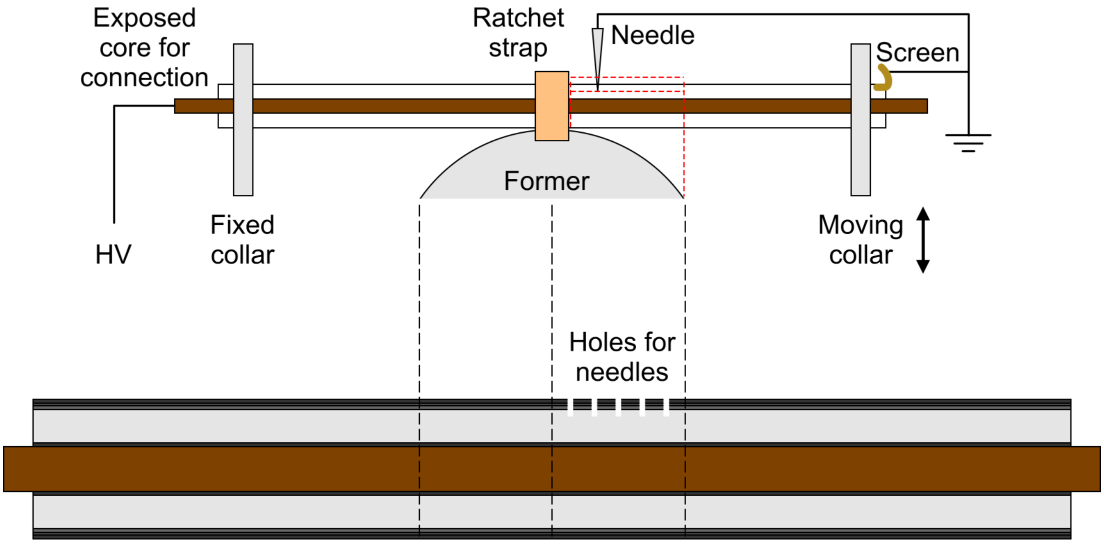

Figure 19. Sketch of cable sample in rig (not to scale). The former has bend radius of 2.5 m, cables were approximately 5 m in length, and needle spacing was 10 cm.

The circuit used is shown in Figure 20. Power was supplied using a Pacific 360-AMX supply and CPTC OC4-0288 NA00206 transformer, protected by a 4.1 kΩ current limiting resistor. Voltage was measured using an AC/DC HV divider CN8552 and calibrated against a Fluke 179 True RMS Multimeter CN8494. The circuit was modelled in LTspice to quantify waveform phase shifting. A high frequency current transformer (HFCT) was used to detect partial discharges to earth and was placed as close to the needle as possible to minimise any antenna effect and electrical noise (Figure 18(j)). Background noise levels could be reduced to approximately 1 pC this way, allowing data signals to be detected (Figure 21). The needle was connected to earth using a fine earth wire and a crocodile clip. The fine wire was cable-tied onto the main cable along its axis to avoid torque on the needle to dislodging during dynamic oscillations on the rig (Figure 18(j)).

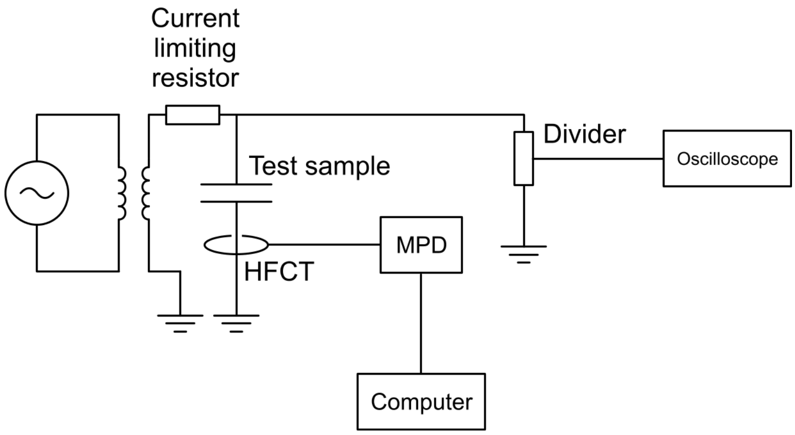

Figure 20. Circuit diagram for large-scale testing

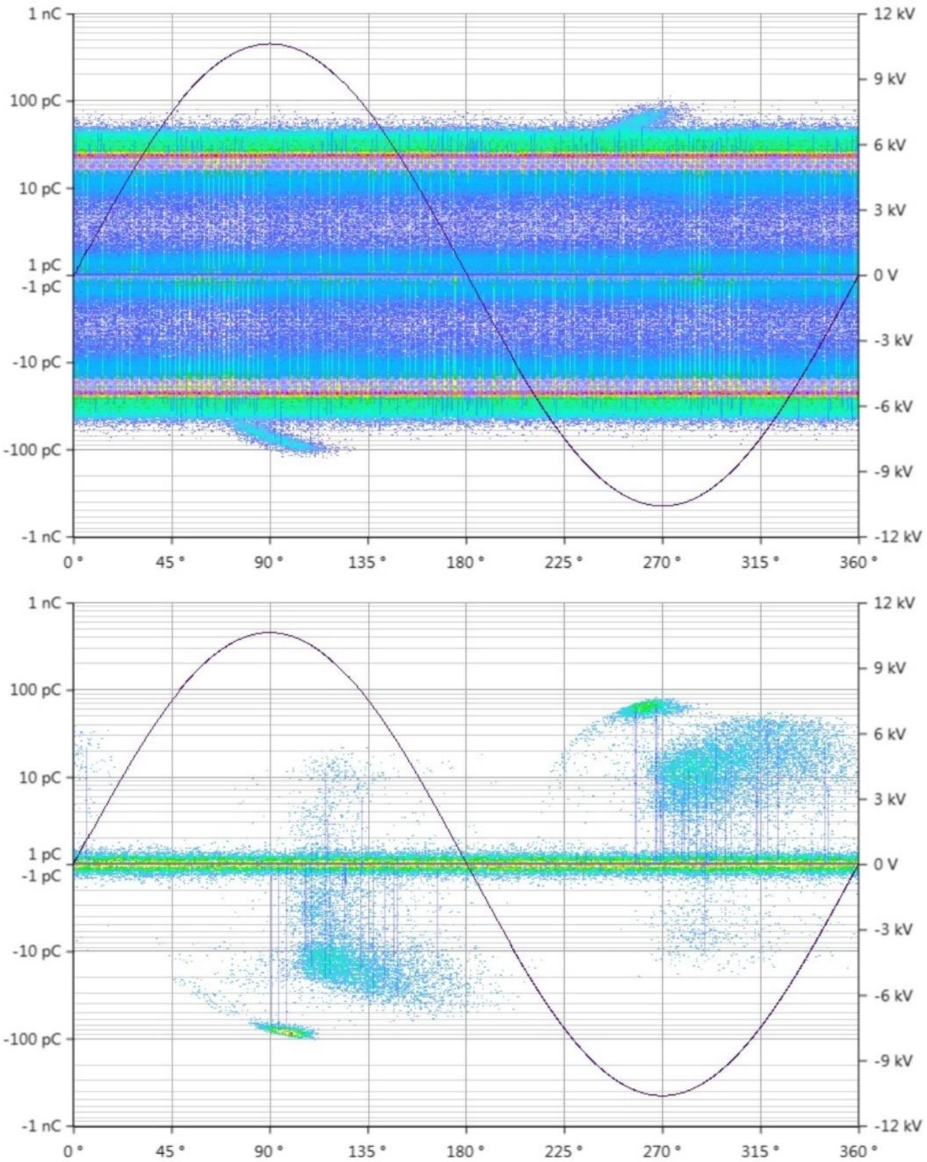

Figure 21. Example of reduction in background electrical noise levels from large bending rig when current transformer is moved as close to the needle as possible to minimise antenna-like noise on earth cable from needle.

Partial discharge charge magnitudes were calibrated against 50 pC pulses across the current transformer. The voltage was increased at approximately 250 V s^{-1} to 7.5 kV_{rms} and partial discharge activity was monitored until tree-like patterns were observed. Trees were allowed to grow for 2 hours, which initial laboratory testing in Manchester suggested allowed sufficient growth in the test cables without breakdown.

Unstrained tests were achieved with a straight cable mounted into the bend rig, whereas static strained tests had the sample bent across the former and held statically. Dynamic bend tests involved the cable flexing between a straight horizontal position to curved across the former at a frequency of 10 Hz. Unstrained and static tests were conducted on the same test sample using multiple holes and needles along the sample above the former region with a spacing of 100 mm. Field modelling using COMSOL showed field magnitudes dropped by over an order of magnitude at this spacing and were thus unlikely to couple (Figure 22). Supplementary empirical testing showed that floating needles did not initiate trees nor allowed continued tree growth after initiation. Only a single needle was used per sample of dynamic testing because of the possibility of tree damage if flexed repeatedly after creation. Post-testing, needles were removed, and sections of the test samples were cut out and polished down to a physical size allowing examination under the microscope.

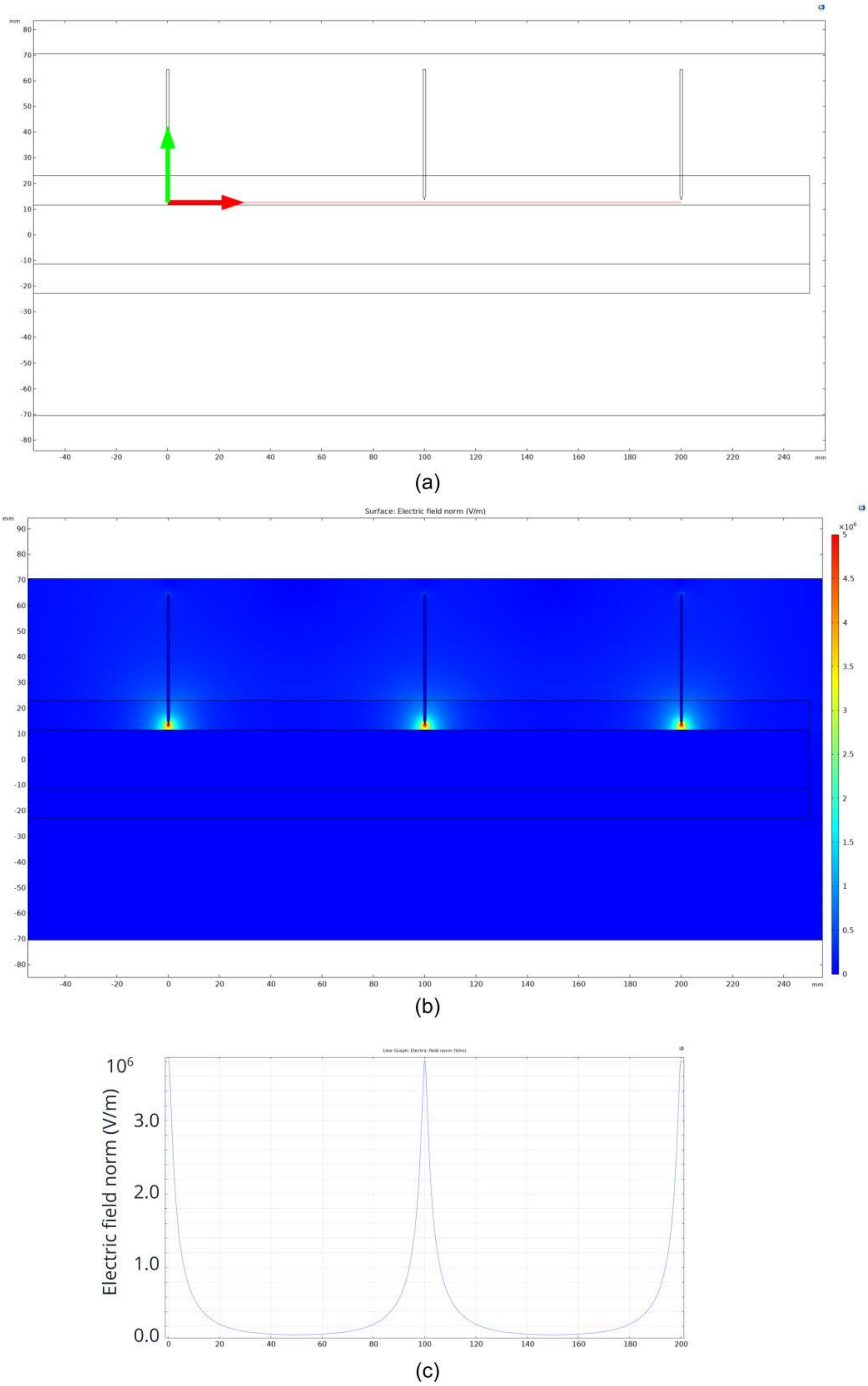

Figure 22. COMSOL modelling of peak electric field strength associated with needles 100 mm apart. (a): Geometry; (b): Electric field strength (kV mm^{-1}), (c): Electric field strength profile between needles about horizontal red line in (a).

4.2 Early results

Initial identical experiments were conducted in the Manchester laboratory on short 10 cm lengths of the same cable used in the larger scale testing (Figure 23). These tests were designed to understand the typical partial discharge behaviour observed under unstrained conditions. Observations showed typical partial discharge behaviour that was comparable to that observed in Figure 17 for extracted XLPE samples. During large scale testing, unstrained samples were tested first to examine any differences that might be introduced by the large rig. Partial discharge behaviour for unstrained samples was very similar to that observed on the short test samples, confirming that no additional complications were being introduced by the large rig. Five static strained tests were then conducted, revealing partial discharge behaviour that was similar to expectation, but also suggested the presence of voids in the system. The pattern that evolved was also atypical, sometimes with longer initiation times and transitions between phases. While patterns showed no features that hadn't been observed before, it is most likely that variations in needle-core gap size, which were inherently difficult to control on the large scale in unsectioned cables, were responsible. Many of the dynamic tests resulted in failure or were rejected, either due to lack of initiation, or sample breakdown, suspected to be caused, again, by gap distances being too large or small. The tests which were successful showed generally similar partial discharge evolution to expectation, with minor deviations again being most likely attributable to gap size and other differences inherently difficult to control on large cables, relative to laboratory samples (Figure 24). Microscopy, which is currently being undertaken in Manchester, is expected to reveal further information.

Figure 23. Offcuts of main samples were prepared into smaller samples for laboratory testing and end-cap design to learn how to minimise electrical noise.

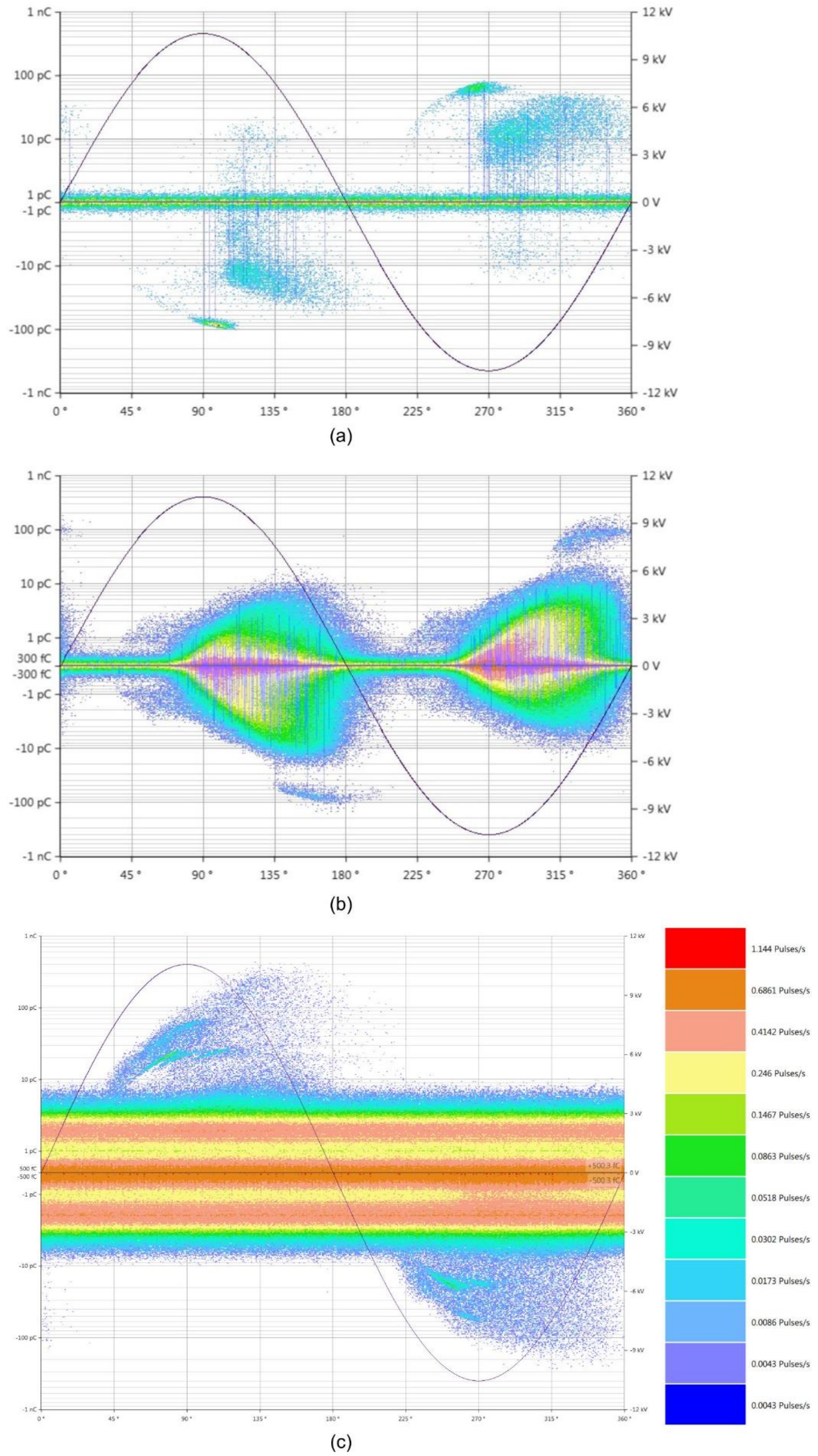

Figure 24. Typical examples of partial discharge activity from dynamic testing on large bend rig. (a) and (b): Example dynamic test partial discharge behaviour analogous to Figure 17 (a) and (c) with additional void-like and additional partial discharge features; (c) A second example of a dynamic test showing more characteristic behaviour analogous to Figure 17 (a).

5 Conclusions

A range of testing at different scales has been conducted to examine whether repeated flexing of a cable significantly reduces the cable's life expectancy through repeated extension and compression of the polymer dielectric, with particular focus on the impact of dynamic strain on electrical tree growth. The results so far acquired have been presented, with testing under DC voltages remaining as future work, and the full-scale AC test analysis is ongoing.

Quantifying the change in volume conductivity of polyethylene as a function of applied tensile strain was a difficult challenge, since the measurement had not been done before, and it was not clear whether data would emerge. As such, the outcome is important. Observations showed no relationship between levels of strain an order of magnitude greater than likely seen in cables in service and the volume conductivity of the dielectric. While mechanical motion may still contribute to failures and to changes in tree inception and growth via other mechanisms, changes in tensile stress do not significantly influence volume conductivity, eliminating this as a potential explanation. The data does not support the hypothesis that the presence of mechanical motion under DC fields is equivalent to an AC field, known to be more aggressive to electrical tree growth. There may be no additional concern from mechanical motion under DC on the field-driven effects of treeing from conductivity changes. However, while it is likely that sample thicknesses were great enough to represent bulk rather than interfacial properties hindered by space charge presence, further investigation is required to confidently establish this. Furthermore, mechanical strain may influence space charge injection, and is a measurement worth making in a future investigation given the electric field strength used in the tests presented here of 10 kV mm^{-1} is half that typically present in HVDC cables.

The application of tensile strain was observed to influence the geometry of electrical trees. Their circumferential spread or width and branch tortuosity reduced with strain when levels exceed 2%. No evidence was observed to indicate tensile strain influenced tree initiation time, growth rate, branch density, or associated partial discharge behaviour. Other forms of strain, such as compressive, torsion, or shear were not examined. Partial discharge behaviour was characteristic and repeatable, typically evolving through three distinct stages during tree development that are not correlated with the physical tree growth. After the initial growth when growth rate stagnates, partial discharge of magnitudes seen initially was not required for significant tree growth.

Early observations from large scale testing on complete cable samples in a large bending rig suggest electrical treeing behaviour typical of that seen at smaller scale. In tests where deviations occurred, these were limited to fine detail in the partial discharge signature and evolution and no new or fundamentally different behaviour was observed. Such deviations are most likely attributed to difficulties in precisely controlling key parameters during testing that are inherent and unavoidable at larger scales. The evidence gathered suggested that small scale laboratory testing is wholly representative of what is observed at larger scales.

References

[1] R. James *et al.*, "Floating Wind Joint Industry Project Phase I Summary Report," May 2018.

[2] Subsea World News, "Industry Teams up to Reduce Offshore Wind Cable Failure Costs.," *https://www.offshore-energy.biz/industry-teams-up-to-reduce-offshore-wind-cable-failure-costs/*, 2018.

[3] J. Su, B. Du, J. Li, and Z. Li, "Electrical tree degradation in high-voltage cable insulation: progress and challenges," *High Voltage*, vol. 5, no. 4, pp. 353–364, Aug. 2020, doi: 10.1049/hve.2020.0009.

[4] L. A. Dissado, S. J. Dodd, J. V. Champion, P. I. Williams, and J. M. Alison, "Propagation of electrical tree structures in solid polymeric insulation," *IEEE Transactions on Dielectrics and Electrical Insulation*, vol. 4, no. 3, pp. 259–279, Jun. 1997, doi: 10.1109/94.598282.

[5] E. Ildstad and S. Hagen, T, "Electrical Treeing and Breakdown of Mechanically Strained XLPE Cable Insulation.," in *1992 IEEE International Symposium on Electrical Insulation*, Jun. 1992, pp. 135–139.

[6] J. v. Champion, S. J. Dodd, and G. C. Stevens, "An examination of the effect of mechanical stress on electrical breakdown in synthetic resin insulators," *J Phys D Appl Phys*, vol. 27, no. 1, pp. 142–147, Jan. 1994, doi: 10.1088/0022-3727/27/1/022.

[7] M. Danikas, D. Papadopoulos, and S. Morsalin, "Propagation of Electrical Trees under the Influence of Mechanical Stresses: A Short Review," *Engineering, Technology & Applied Science Research*, vol. 9, no. 1, pp. 3750–3756, Feb. 2019, doi: 10.48084/etasr.2483.

[8] E. David, J.-L. Parpal, and J.-P. Crine, "Influence of internal mechanical stress and strain on electrical performance of polyethylene electrical treeing resistance," *IEEE Transactions on Dielectrics and Electrical Insulation*, vol. 3, no. 2, pp. 248–257, Apr. 1996, doi: 10.1109/94.486777.

[9] S. Boggs, D. H. Damon, J. Hjerrild, J. T. Holboll, and M. Henriksen, "Effect of insulation properties on the field grading of solid dielectric DC cable," *IEEE Transactions on Power Delivery*, vol. 16, no. 4, pp. 456–461, 2001, doi: 10.1109/61.956720.

[10] BS-6233:1982, "Methods of test for volume resistivity and surface resistivity of solid electrical insulating materials." BSI Standards Publication, p. 13, 1982.

[11] B. X. Du, Z. R. Yang, Z. L. Li, and J. Li, "Temperature-dependent nonlinear conductivity and carrier mobility of silicone rubber/SiC composites," *IEEE Transactions on Dielectrics and Electrical Insulation*, vol. 25, no. 3, pp. 1080–1087, Jun. 2018, doi: 10.1109/TDEI.2018.006942.

MANCHESTER 1824
The University of Manchester

[12] P. Dhima and F. Vila, “Determination of Volume Conductivity of Polyethylene Using Positive Corona, When the Current through the Sample Depends Linearly on Grid Potential,” *Journal of Materials Science and Chemical Engineering*, vol. 05, no. 12, pp. 40–51, 2017, doi: 10.4236/msce.2017.512004.

[13] F. Vila, G. M. Sessler, and H. Sykja, “The influence of electron-beam irradiation on the volume resistivity of polyethylene and kapton,” *J Electrostat*, vol. 63, no. 6–10, pp. 749–754, Jun. 2005, doi: 10.1016/j.elstat.2005.03.039.

[14] R. A. Moreno and B. Gross, “Measurement of potential buildup and decay, surface charge density, and charging currents of corona-charged polymer foil electrets,” *J Appl Phys*, vol. 47, no. 8, pp. 3397–3402, Aug. 1976, doi: 10.1063/1.323199.

[15] R. W. Warfield and M. C. Petree, “Electrical resistivity of polymers,” *Polym Eng Sci*, vol. 1, no. 2, pp. 80–85, Apr. 1961, doi: 10.1002/pen.760010208.

[16] L. K. H. Pallon *et al.*, “Formation and the structure of freeze-dried MgO nanoparticle foams and their electrical behaviour in polyethylene,” *J Mater Chem A Mater*, vol. 3, no. 14, pp. 7523–7534, 2015, doi: 10.1039/C4TA06362G.

[17] G. Chen, J. Zhao, S. Li, and L. Zhong, “Origin of thickness dependent dc electrical breakdown in dielectrics,” *Appl Phys Lett*, vol. 100, no. 22, p. 222904, May 2012, doi: 10.1063/1.4721809.

[18] J. H. Mason, “Breakdown of solid dielectrics in divergent fields,” *Proceedings of the IEE Part C: Monographs*, vol. 102, no. 2, p. 254, 1955, doi: 10.1049/pi-c.1955.0030.

[19] IEC 60270, “High-voltage test techniques — Partial discharge measurements,” 2000.

[20] K. Kudo, “Fractal analysis of electrical trees,” *IEEE Transactions on Dielectrics and Electrical Insulation*, vol. 5, no. 5, pp. 713–727, 1998, doi: 10.1109/94.729694.

[21] B. X. Du, J. G. Su, and T. Han, “Compressive stress dependence of electrical tree growth characteristics in EPDM,” *IEEE Transactions on Dielectrics and Electrical Insulation*, vol. 25, no. 1, pp. 13–20, Feb. 2018, doi: 10.1109/TDEI.2018.006593.

[22] W. Jiaxing, M. Siping, and X. Man, “Effect of Large Mechanical Stress on Electrical Tree Characteristics of Silicone Rubber,” in *Proceedings of the IEEE International Conference on Properties and Applications of Dielectric Materials*, Jul. 2021, vol. 2021-July, pp. 143–146. doi: 10.1109/ICPADM49635.2021.9493916.